A crack growth rate model with load history effects for mode I fatigue-driven delamination under multi-level block loading

Jensen, S.M.; Carreras, L.; Bak, B.L.V.; Lequesne, Cedric; Lindgaard, E.

Published in:
International Journal of Fatigue

DOI (link to publication from Publisher):
10.1016/j.ijfatigue.2023.107595

Publication date:
2023

Document Version
Publisher's PDF, also known as Version of record

International Journal of Fatigue 172 (2023) 107595

Contents lists available at ScienceDirect

International Journal of Fatigue

journal homepage: www.elsevier.com/locate/ijfatigue

A crack growth rate model with load history effects for mode I fatigue-driven delamination under multi-level block loading

S.M. Jensen [a,*], L. Carreras [a], B.L.V. Bak [a], C. Lequesne [b], E. Lindgaard [a]

[a] The CraCS research group, Department of Materials and Production, Aalborg University, Fibigerstraede 16, DK-9220, Aalborg East, Denmark[1]
[b] Siemens Digital Industries Software, Simulation and Test Solution, Rue des Chasseurs Ardennais 8, Angleur 4031, Belgium

ARTICLE INFO

Dataset link: http://dx.doi.org/10.17632/gj69dy4pcp.1

Keywords:
Fiber reinforced polymer materials
Fatigue delamination
Variable amplitude loading
Energy release rate control
Crack growth rate model

ABSTRACT

Load interaction effects in fatigue-driven delamination in fiber-reinforced polymer composites are neglected in state-of-the-art models although this assumption highly underestimates the delamination growth under variable amplitude (VA) loading. A new phenomenon called "transient delamination growth" has recently been observed in VA fatigue experiments by the authors. In the current work a new crack growth rate model with transient delamination growth capabilities is presented. The new model evaluates the crack growth rate by addition of a steady-state non-interaction term and a transient interaction term. The former term neglects load interaction effects and is characterized from constant amplitude loading tests, while the latter term includes load interaction effects and is characterized from two-level block loading tests. Fatigue tests are conducted on glass/epoxy DCB specimens by means of a new test fixture. The new crack growth rate model is able to accurately represent the crack growth rate at high-to-low load amplitude changes during multi-level block loading tests and reduces the error in delamination growth prediction by nearly 50% compared to non-interaction models.

1. Introduction

Delamination (interlaminar cracking) is a failure mode of particular concern in laminated fiber reinforced polymer (FRP) composite structures. For example, delaminations are critical in wind turbine blades (WTB) and often leads to ultimate failure, e.g. through an interacting process of delamination and buckling leading to structural collapse [1]. Most structural designs of WTBs follow a conservative "no growth" philosophy and do not consider the progressive interlaminar failure [2]. This hinders innovative designs and may underestimate the actual material properties, e.g. due to toughening mechanisms such as fiber bridging [2,3]. Additionally, composite structures mostly undergo variable amplitude (VA) loading spectra during operation, which introduce many difficulties from a modeling perspective as summarized in [4]. A major challenge is that composite material fatigue damage accumulation is highly sensitive to load interaction effects [5,6], i.e. the current damage growth increment depends on the load history. The majority of experimental studies on VA fatigue of composites investigates the number of load cycles to failure or the residual macroscopic specimen properties [7,8], such as the residual strength [9–11] or residual stiffness [12]. Few studies investigate the progression of actual damage mechanisms under VA loading, such as matrix cracking [13–17], delamination [18–22], or adhesive debonding cracks [18,23,24], which provide insightful experimental observations for development of mechanistic damage models, cf. the definition in [4,25].

Several models have been developed for fatigue life prediction of FRPs under VA loading. Examples of this are damage accumulation rules and residual strength and residual stiffness-based models [26,27]. However, research mostly focus on VA fatigue in un-notched FRP composite specimens.

Delamination growth during two-level block loading, i.e. a block loading spectrum that consists of multiple constant amplitude (CA) load blocks with two different amplitude and mean values, is investigated in [18–22] using double cantilever beam (DCB) specimens in mode I crack opening. In [19–21] load sequence experiments are conducted to investigate delamination growth during a single high-to-low and/or low-to-high step change in the cyclic maximum load or the load ratio. The results prove a significant dependence of the load history on the delamination growth rate. The experimental studies in [18,20,22] investigate delamination growth during two-level block loading spectra with periodic repeated high (H) and low (L) load blocks. Generally,

* Corresponding author.
E-mail addresses: smj@mp.aau.dk (S.M. Jensen), lcb@mp.dk (L. Carreras), brianbak@mp.aau.dk (B.L.V. Bak), cedric.lesquesne@siemens.com (C. Lequesne), elo@mp.aau.dk (E. Lindgaard).
[1] http://www.www.cracs.aau.dk

https://doi.org/10.1016/j.ijfatigue.2023.107595
Received 28 October 2022; Received in revised form 10 February 2023; Accepted 24 February 2023
Available online 7 March 2023

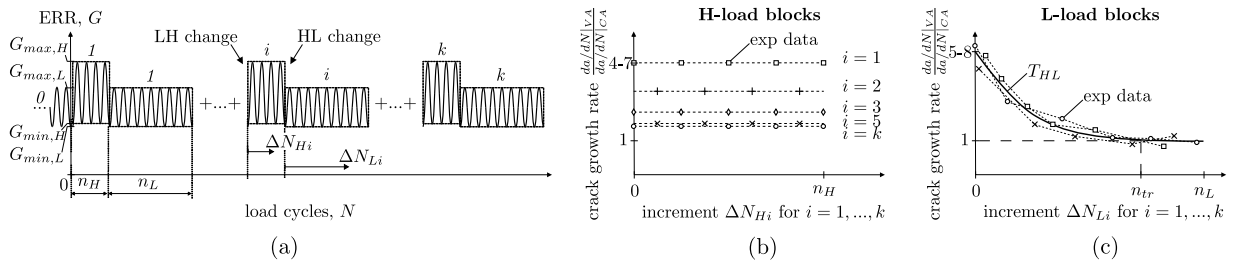

Fig. 1. Graphical summary of experimental results from two-level block loading tests on transient crack growth rates following load amplitude changes [22]. (a) Two-level block loading test with periodic repeated changes in load amplitude level between a low (L) load level and a high (H) load level. (b) Transient response in the crack growth rate after LH load amplitude changes. (c) Transient response in the crack growth rate after HL load amplitude changes.

an increased crack extension is observed in comparison to Paris' law-based predictions using CA baseline data. The crack extension increases particularly when frequent load amplitude changes occur [22].

Finally, the experimentally observed load interaction effects for fatigue-driven delamination are not accounted for in state-of-the-art prediction models [28], which means they yield highly non-conservative results for VA loading. To the best of the authors' knowledge, the current work presents the first fatigue-driven delamination model that accounts for load interaction effects in FRP laminates when subjected to VA loading.

1.1. Summary on transient delamination growth

The research questions addressed in this work build on previous experimental work by the authors [22], for which reason a brief summary is provided here. The experiments are VA cyclic tests on DCB specimens with real-time control of the applied energy release rate (ERR), G. The applied load patterns consist of repeated H- and L-load blocks as illustrated in Fig. 1(a). High precision measurements of the crack front position ($\sim$ 0.01 mm) during two-level block loading enabled the authors to observe a transient delamination growth phenomenon, which is a transient phase that follows load amplitude changes in VA load spectra. In the transient phase a significantly increased crack growth rate, da/dN_{VA}, is measured compared to CA baseline measurements, da/dN_{CA}. In the following, the term "CA loading" will refer to a cyclic varying ERR, G, with constant maximum and minimum values, G_{max} and G_{min}, respectively. The term "load amplitude change" refers to a step change in amplitude of the cyclic ERR. The terms low-to-high (LH) and high-to-low (HL) load amplitude changes are defined and illustrated in Fig. 1(a).

The main experimental observations and trends on transient crack growth in [22] have been summarized in the following list and Fig. 1(b)–(c). Notice, that prior to the first H-load block the DCB specimens are subjected to CA loading (block no. 0) with loading conditions identical to the L-load blocks of the block loading spectrum. The initial CA loading is continued until the fracture process zone is fully developed.

(a) The crack growth rates, $da/dN|_{VA}$, are significantly higher in the majority of the H- and L-load blocks of the VA tests in comparison to the CA baseline, $da/dN|_{CA}$.
(b) A higher crack growth rate is measured during the early H-load blocks (e.g. load block no. 1–3) of the two-level block loading test compared to the crack growth rate measured during later H-load blocks (e.g. load block no. ≥ 4), see Fig. 1(b).
(c) The short duration of the H-load blocks in the two-level block loading tests ($n_H = 200$ cf. Fig. 1(a)) makes it impractical to characterize a transient phase following the LH load amplitude change. However, experiments with a single LH load amplitude change prove a transient response in the crack growth rate that initially overshoots and eventually approaches the CA baseline measurements as the number of load cycles increases.
(d) Characteristic responses in the crack growth rates are observed in the L-load blocks. The responses are independent of the load block number, i.
(e) A high crack growth rate is observed for the L-load blocks immediately after the HL load amplitude change, see Fig. 1(c). Typical values are 5 to 8 times higher than $da/dN|_{CA}$. The crack growth rate decreases with increasing number of load cycles. After several thousands of load cycles the crack growth rate returns to the CA baseline, $da/dN|_{CA}$, see n_{tr} in Fig. 1(c).
(g) The effect of frequent load amplitude changes is investigated in two-level block loading tests by halving the duration of the H- and L-load blocks, n_H and n_L, respectively. Frequent load amplitude changes increase the crack extension significantly. The transient response following each HL load amplitude change is the same independent of the tested size of n_H and n_L.

The transient response following the HL load amplitude change is well-suited for characterization due to the observation *(d)* since this allows for repeated measurements on a single specimen. However, since the observations are made for two-level block loading tests with constant values of $G_{max,H}$, $G_{max,L}$, $G_{min,H}$ and $G_{min,L}$, it remains unclear what the effects of changing these quantities are. Further studies on these effects are presented in this work by varying the difference between $G_{max,H}$ and $G_{max,L}$ ($\Delta G_{max} = G_{max,H} - G_{max,L}$).

1.2. Research objectives

In the current work a new crack growth rate model with load interaction capabilities is presented. Load interaction effects are introduced to the model by means of a transient delamination growth phenomenon, which has recently been observed to follow load amplitude changes in fatigue tests on DCB specimens subjected to VA block loading. The proposed crack growth rate model takes the following form:

$$\frac{da}{dN} = \frac{da}{dN}_{ss} + \frac{da}{dN}_{tr} \tag{1}$$

where the current crack growth rate, da/dN, consists of two terms, which will be denoted as the steady-state term, da/dN_{ss}, and the transient term, da/dN_{tr}. The steady-state crack growth rate term, da/dN_{ss}, corresponds to the CA baseline crack growth rate. The transient term, da/dN_{tr}, includes a load history-dependent function that represents the phenomenological characteristics observed experimentally in two-level block loading tests. This is exemplified by the curve T_{HL} in Fig. 1(c).

In the pursuit of formulating the functions for the two terms in Eq. (1), the work has been structured around the following tasks *(A)–(C)*.

(A) Formulate a phenomenological crack growth rate model according to Eq. (1), whose model parameters can be obtained from CA and two-level block loading experiments.
(B) Establish functions (e.g. T_{HL} in Fig. 1(c)) to describe the transient crack growth rate, da/dN_{tr}, and assess the functions' dependence on governing fatigue load parameters.

(C) Demonstrate the capabilities and limitations of the new crack growth rate model in multi-level block loading.

The paper is structured as follows. Section 2 considers item *(A)* and presents the formulation of a new crack growth rate model with transient responses at load amplitude changes. Section 3 explains the experimental methodology for performing two- and multi-level block loading tests and the experimental characterization procedure to determine the transient function related to item *(B)*. The block loading experiments are performed using a new test fixture for mode I fatigue crack growth with real-time control of the applied ERR, which will be introduced in Section 3.2. Section 4 presents an application of the new crack growth rate model to a multi-level block load test, which serves to demonstrate the capabilities and limitations of the proposed model (item *(C)*). A discussion of the results are included in Section 5 and finally Section 6 concludes the work and revisits the items *(A)–(C)* as listed above.

2. An interaction crack growth rate model

Before the new crack growth rate model with load interaction effects is described, a brief summary of the conventional non-interaction model is included.

2.1. Conventional non-interaction model

A crack growth prediction can be obtained by direct summation of crack increments caused by each load cycle. A common approach is to assume that the crack growth increment, Δa_i, associated with a given load cycle, N_i, of variable amplitude loading can be estimated from CA data and a Paris' law relation $F(G_{max}, R)$:

$$a_N = a_0 + \sum_{i}^{N_{tot}} \Delta a_i = a_0 + \sum_{i}^{N_{tot}} F(G_{max,i}, R_i) \tag{2}$$

where a_0 is the starting crack length, N_{tot} is the total number of load cycles and a_N is the crack length after N_{tot} load cycles. This model assumes that the current crack increment can be evaluated from the instantaneous value of the cyclic load parameters $(G_{max,i}, R_i)$ at a given load cycle, N_i. This type of model is also known as a non-interaction model as load interaction effects are neglected. Most state-of-the-art prediction models for delamination in FRP composites are based on fracture mechanics and/or damage mechanics [28] in a cohesive zone modeling framework [29–36]. Many of the fatigue cohesive zone models in finite element formulations rely on a non-interaction model and thereby neglect load interaction effects [37–52]. The conventional non-interaction model will be benchmarked against the new crack growth rate model and experimental data from multi-level block loading tests in later sections.

2.2. Crack growth rate model with load interaction

The new crack growth rate model includes transient responses in the crack growth rate at load amplitude changes. This is ensured by activating a function for the transient response when step changes in the maximum applied ERR, G_{max}, occurs. Load amplitude changes in a VA load spectrum will either be a LH type or a HL type. Section 1.1 concludes that the transient responses following HL load amplitude changes in two-level block loading are significant and well-suited for characterization. The responses at LH load amplitude changes are less suited for characterization due to item *(b)*. As a result, the new crack growth rate model will neglect the transient crack growth rate at LH load amplitude changes, and solely focus on the transient crack growth rate at HL load amplitude changes. The consequence of this will be addressed in later sections.

Recall Eq. (1). The steady-state term is a non-interaction term because the current value depends only on the instantaneous values of the cyclic load parameters, such that the term can be evaluated from a Paris' law-like relation, $F(G_{max}, R)$. The transient term, da/dN_{tr}, is zero by default and becomes non-zero if a HL load amplitude change has occurred. The transient term goes to zero with an increasing number of load cycles. The transient term depends on the current cyclic load parameters and the load history, i.e. the term is an interaction term. This has been summarized in the following two equations for computation of the steady-state and transient terms, respectively:

$$\frac{da}{dN}_{ss} = F(G_{max}, R) \tag{3}$$

$$\frac{da}{dN}_{tr} = \begin{cases} T_{HL} & \text{for cond. I} \\ 0 & \text{for cond. II} \end{cases} \tag{4}$$

where the transient term will attain one of the two functions in Eq. (4) depending on the following conditions I and II:

(I) Condition I: Crack growth following a HL load amplitude change.
(II) Condition II: Any other case. Including crack growth following a LH load amplitude change.

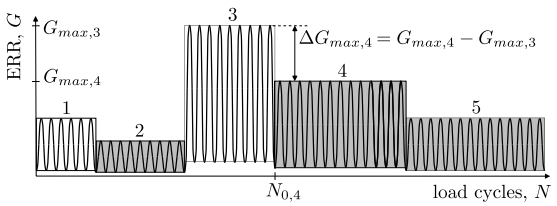

Fig. 2. The transient term will be non-zero in the gray load blocks of this example. Note also the definition of N_0 and ΔG_{max} for load block number 4.

The conditions are illustrated in a multi-level block load spectrum in Fig. 2. The transient function, T_{HL}, will apply the experimental trends derived from two-level block loading tests. The transient function, T_{HL}, for the HL load amplitude change is assumed to be an exponential decay function of the following form:

$$T_{HL} = B \exp\left(-\frac{\Delta N}{\tau}\right) \frac{da}{dN}_{ss} \tag{5}$$

The transient function in Eq. (5) depends on the load cycle increment $\Delta N = N - N_0$ where N_0 is the number of load cycles at which the HL load amplitude change occurred. The parameter B is a unit-less scaling parameter that represents the initial overshoot in the transient crack growth rate (i.e. when $\Delta N = 0$) relative to the CA baseline value, da/dN_{ss}. The steady-state crack growth rate, da/dN_{ss}, is evaluated according to a Paris' law-like relation (Eq. (3)). The decay constant, τ, has units of load cycles, and determine the rate of decay of the transient function. The transient function in Eq. (5) depends explicitly on the number of load cycles, and the instantaneous fatigue load quantities, G_{max} and R through Eq. (3). The parameters B and τ will depend on further fatigue load quantities, such as the step change in ERR, $\Delta G_{max} = G_{max,H} - G_{max,L}$, as explained further in later sections.

The new crack growth rate model assumes a block-wise definition of the applied load spectrum, however, the load blocks may have any duration. The transient term will reset when a new load block is encountered. The approach as presented here is most suited for multi-level block loading spectra or VA load spectra that can be naturally divided into multi-level block loading spectra (may require pre-processing of the VA load spectra).

A simple one-dimensional crack growth prediction can be computed by integration of Eq. (1) with substitution of Eq. (3) to Eq. (5). For example, assume a HL step change in load amplitude has occurred at $N = N_0$ (e.g. from load block no. 3 to 4 in Fig. 2), then the crack extension during the current load block can be described by

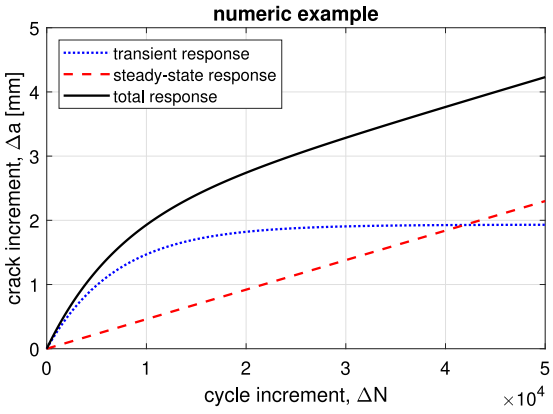

Fig. 3. Numeric example to illustrate the crack growth after a HL load amplitude change. Parameters used in the example: $B = 6$, $\tau = 7000$, $G_{max}/G_c^{ss} = 0.3$, $R = 0.2$, Paris' law parameters: $A = 0.0727$, $p = 5.13$.

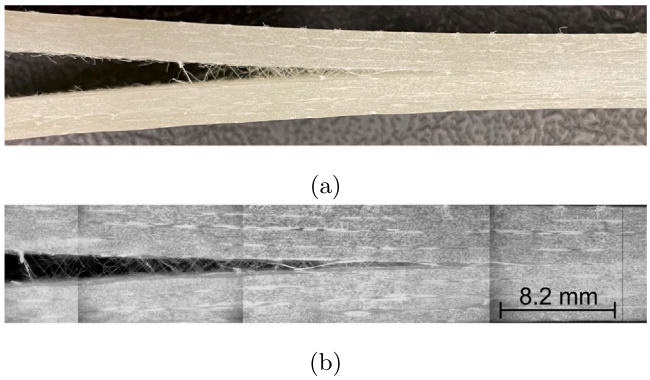

Fig. 4. The DCB specimen and its' fully developed fiber bridging zone. The photos are taken through a digital camera and a microscope (at magnification level 2.0x and approximate imaging distance of 240 mm) in Fig. (a) and (b), respectively. Focus stacking is applied in Fig. (b).

the following expression (the parameters B and τ are constants in the integration with respect to N for the current load block):

$$\Delta a = \frac{da}{dN}_{ss} \left((N - N_0) + B\tau \left(1 - \exp\left(-\frac{N - N_0}{\tau} \right) \right) \right) \tag{6}$$

A numeric example is included in Fig. 3, which clearly illustrates the effect of the transient response on the crack length prediction. A similar procedure is implemented in a MATLAB program to perform simple one-dimensional predictions of crack growth during multi-level block loading in ERR control. The results will be presented in Section 4.

3. Experimental methodology

An experimental campaign is carried out with two purposes: Firstly, to characterize the transient function, T_{HL}, from two-level block loading tests. Secondly, to generate a multi-level block loading test for demonstration of capabilities and limitations of the new crack growth rate model.

3.1. Material and specimen

The test campaign uses double cantilever beam (DCB) specimens. The DCB specimens are made of glass fiber reinforced epoxy. The glass fiber mats consist of unidirectional fiber bundles in a non-crimp fabric architecture with backing fibers in the ±45° directions, and fiber bundle stitching yarns. The areal weight of the fiber mats is 1483 kg/m^2 with 7 wt% backing fibers. The material is widely used in the WTB industry. The specimens are manufactured by VARTM. The DCB specimens have the following nominal dimensions: Length $L = 657$ mm, total height $2H = 8.2$ mm and width $w = 27.8$ mm. The artificial pre-crack has a nominal length of $a_0 = 100$ mm, which has been introduced in the laminate by placing a 13 μm thick poly-tetrafluoroethylene (PTFE) film in the layup. The Young's modulus in the fiber direction is $E = 37.2$ GPa. The delamination propagates along a UD 0°/0° interface. The mode I fracture toughness (plateau value) is $G_c^{ss} = 1359$ J/m^2. Photos of the fiber bridging zone is shown in Fig. 4. Microscopy inspections of the fracture surfaces show that the fiber bridging zone is primarily made up by stitching yarns.

3.2. Test rig for ERR-controlled cyclic testing

The experimental test campaign applies a novel ERR-controlled fatigue version of the pure moment loaded double cantilever beam (DCB) test. The applied bending moments, M, at the upper- and lower DCB arms are equal in magnitude but have opposite signs such that the delamination propagates under pure mode I crack opening. The path independent J-integral can be applied to compute the ERR accounting for large-scale bridging conditions (i.e. when the size of the fiber bridging zone, L_{pz}, is comparable to the specimen's dimensions). The following equation applies for an orthotropic laminate (plane stress) and mode I crack opening [53–55]:

$$G = J = \frac{M^2}{W E_1 I} \tag{7}$$

where E_1 is Young's modulus in the specimens longitudinal direction (i.e. fiber direction), W is the specimen width, I is the area moment of inertia of the DCB arms ($I = 1/12 W H^3$), and M is the applied bending moment as illustrated in Fig. 5. Note that the applied ERR, G, is independent of the crack length, a, and does neither depend on the magnitude nor the distribution of bridging tractions in the wake of the crack tip. Additionally, the applied ERR, G, is directly proportional to the squared value of the applied bending moment, M^2. Therefore, an M-controlled cyclic test is equivalent to a ERR-controlled cyclic test using the current test specimen configuration.

The basic operating principle of the new test fixture is schematically shown in 2D in Fig. 5, and a photograph of the test fixture is shown in Fig. 6. The test fixture uses the same basic principle as the test fixture developed in [56], however, modifications are necessary to enable cyclic testing of compliant DCB specimens, e.g. laminated GFRP DCB specimens, in ERR-control. The modifications will be described in the remaining of this subsection.

Pure bending moments are applied to the DCB specimen through a wire pulley system as illustrated in Figs. 5 and 6. The load string comprises the DCB specimen, a dynamic 2kN rated Instron load cell, the upper- (radius $R = 60.0$ mm) and lower (radius $r = 40.0$ mm) wheels, four Teflon-coated steel wires of diameter d=1.1 mm, and two loading blocks, which are directly attached to the tabs of the DCB specimen. The upper wheels are attached to a linear actuated piston from a computer-controlled electric Instron test machine (E10000 system). The lower wheel is kept fixed and directly connected to the load cell, which is attached to the load frame table of the test machine as shown in Fig. 6. The upper- and the lower wheels may rotate with negligible friction using low friction hybrid ceramic bearings. A support structure is installed to ensure that the longitudinal center axis of the DCB specimen remains horizontal as the piston translates. The test machine's crosshead displacement is equal to the displacement of the upper wheels, which will be denoted by v in the following. The rotations of the upper- and lower loading blocks are symmetric and the angles of rotation will be denoted by θ. The applied bending moment, M, is comprised of the force couples of magnitude, $F/2$, where F is the force measured by the load cell, see Fig. 5. The moment arm of the force

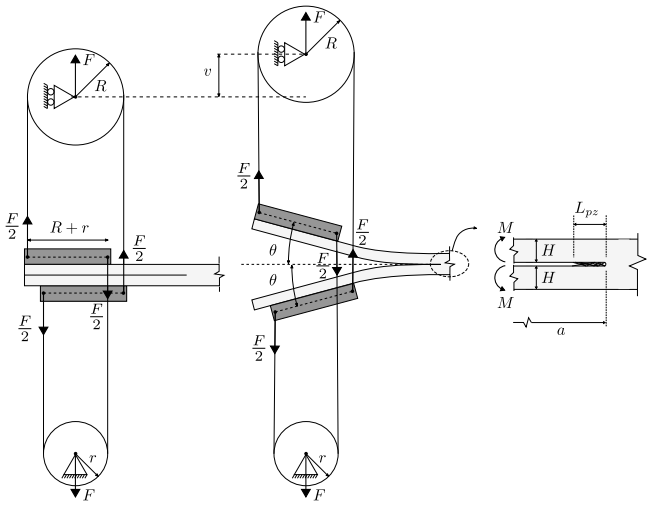

Fig. 5. Schematic outline of the load introduction to the pure moment loaded DCB specimen.

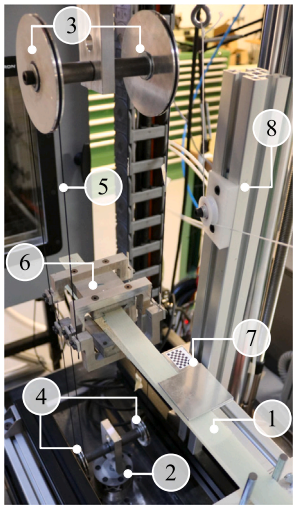

Fig. 6. Photography of the test fixture. Annotations: 1: DCB specimen; 2: Load cell; 3: upper wheels; 4: Lower wheels; 5: Teflon coated steel wire; 6: Loading blocks; 7: Checkerboard pattern; 8: Specimen support structure.

couple reduces as the DCB arms rotate, which is illustrated in Fig. 5 and by the following equation:

$$M = \frac{F(R+r)}{2}\cos\theta = \frac{F(R+r)}{2} f(v) \tag{8}$$

The applied bending moment becomes a function of the angle of rotation, θ, and the applied force, F, i.e. $M(F,\theta)$. A simple kinematic relation can be derived between the angle of rotation, θ, and the displacement, v: $\theta = p(v)$, such that the applied bending moment can be rewritten to be a function of the form seen on the right-hand side in Eq. (8), i.e. $M(F,\theta) \Rightarrow M(F,v)$, where $f(v) = \cos(p(v))$.

The kinematic relation $p(v)$ is derived from an experiment of simultaneous measurements of the cross head displacement, v, and the angle of rotation, θ, which has been measured using an inclinometer. The measurements are shown in Fig. 7(a). A second order polynomial curve fit is generated using the following parameters:

$$p(v) = p_0 + p_1 v + p_2 v^2 \tag{9}$$

$$p_0 = 8083; p_1 = 835.7; p_2 = -0.1023; R^2 = 0.99$$

The curve fit is based on a suitable range of the displacement $v \in [0; 20]$ mm that may be experienced in the cyclic tests. The relation

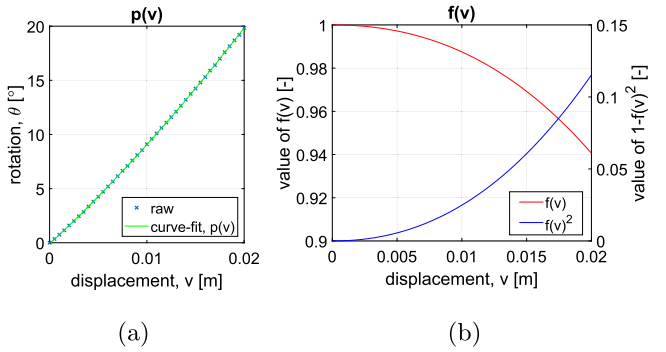

Fig. 7. (a) Kinematic relations to establish a relation between the cross head displacement and the angle of rotation. (b) Graphs for $f(v) = \cos(p(v))$ and $\epsilon = 1 - f(v)^2$.

applies for the current test fixture configuration and is independent of the crack length. Substitution of Eq. (8) in Eq. (7) yields the following equation for the applied ERR, G:

$$G(F,v) = \frac{1}{BE_1 I}\left(\frac{F(R+r)}{2}\right)^2 f(v)^2 \tag{10}$$

where $f(v) = \cos(p(v))$. Fig. 7(b) shows graphs for the functions $f(v)$ and $\epsilon = 1 - f(v)^2$ on the left and right axis, respectively. The value $\epsilon = 1 - f(v)^2$ is the error introduced on G if the changing moment arm as the loading blocks rotate is neglected, i.e. assuming that $M(\theta, v) \approx M(F)$. For example, an error of $\epsilon = 5\%$ and $\epsilon = 10\%$ in the applied ERR, G, will be encountered for a cross head displacement of $v = 13.7$ mm and $v = 18.5$ mm, respectively. This error has a significant effect on the crack growth rate due to the typical power-relation between da/dN and G, and therefore the angle of rotation, θ, should be taken into account.

To perform M-controlled cyclic tests, the controller of the test machine needs to generate a controllable channel similar to Eq. (8) by combining signals from two physical source transducers: The force transducer to measure F and the position transducer to measure v. This is accomplished using user-defined Channel Calculations and Advanced Amplitude Control options in the *Instron WaveMatrix2* software.

3.3. ERR-controlled VA testing

The test fixture is be applied for VA loading such that the applied bending moment, M, (equivalently the ERR, G) is prescribed according to two- and multi-level block loading spectra. The crack growth rate immediately after load amplitude changes is of particular interest in the current work, which makes it relevant to evaluate the controller's ability to reach the target value when changes in loading conditions occur. Fig. 8(a)–(b) shows the relative difference between the target moment and the measured moment following LH- and HL step changes in load amplitude level during a two-level block loading test. Note that within $\Delta N = 20$ cycles the relative difference becomes less than 1%. The target value is reached within $\Delta N = 40$ and $\Delta N = 50$ cycles following the LH and the HL load amplitude change, respectively. Note also that the responses reach the target values from below in both cases.

The relative difference between the target and measured signals has also been investigated during multi-level block loading tests. The results are similar to the response in Fig. 8, and similar responses are observed across all magnitudes of the step change in load level.

3.4. Crack growth rate measurements

The crack length, a, is measured using an automated digital-image based technique that has been developed in [57] for tracking of the crack fronts in translucent materials. The method has been applied in recent studies of fatigue-driven delamination under VA loading

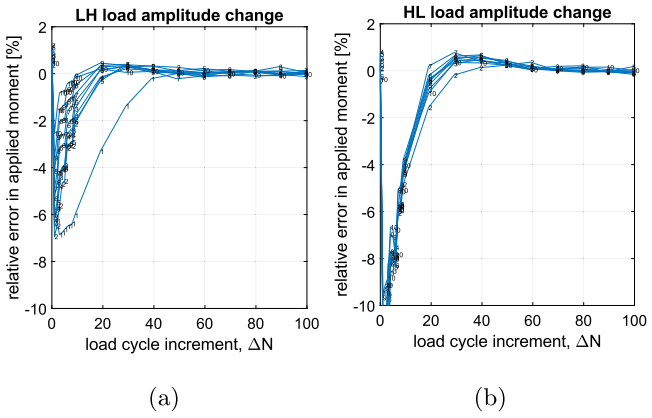

Fig. 8. (a)–(b) The relative error $(((M_{actual} - M_{target})/M_{target}) * 100)$ in the max value of the applied bending moment, M_{max}, following LH load amplitude changes (a) and HL load amplitude changes (b) in a two-level block loading experiment with repeated L- and H-blocks. The number annotations refer to the load block number.

in [21,22]. The setup uses the following hardware: A monochrome FLIR Blackfly CCD type camera with a resolution of 2448 × 2048 pixels, two cool LED white light sources NILA Zaila Daylight to illuminate the top surface of the DCB specimen, and a computer for image acquisition and storage. Images are acquired at a predefined cycle increment, ΔN_{image}, which controls the temporal resolution of the crack length measurements. The process is fully automated and continuous without pausing/interrupting the cyclic test. The crack tracking algorithm outputs the average crack length, a, across the specimen width as a function of the number of load cycles, N. The resolution of the average crack length across the specimen width is 0.05 mm for the current test setup, specimen geometry, and material system. The crack growth rate, da/dN, is computed for every data point in the (N, a)-data set by fitting a linear function to all data points within a moving fitting window that has been centered around the data point of interest [57]. When the applied load pattern is a two- or multi-level block loading type, the crack growth rate, da/dN, is computed separately for every load block.

In all the tests the crack is propagated in fatigue for at least $\Delta a = 20$ mm of crack extension before the crack front reaches the gauge region for the subsequent VA loading tests. During this phase the applied ERR corresponds to the ERR of the first load block in the block loading fatigue test. This procedure is followed to ensure a natural pre-crack and a fully developed fiber bridging zone at the beginning of the gauge region.

3.5. Test programme

An overview of the cyclic tests may be found in Table A.1 in Appendix A. The cyclic tests can be divided into three main types: Constant amplitude tests (denoted by *CA* in the test ID), two-level block loading tests similar to Fig. 1(a) (denoted by *BL* in the test ID), and a multi-level block loading test. The latter test type will serve as a demonstrator test in later sections and the test ID in Table A.1 is therefore denoted by *DEM*. The multi-level block loading test is suitable here as it possesses an increased degree of complexity compared to two-level block loading tests while allowing meaningful measurements of crack growth rate during VA testing. The reader is referred to Table A.2 for further detail on the applied load spectrum for the demonstrator test.

All cyclic tests are performed in ERR-control. The applied ERR will be expressed as a fraction of the fracture toughness of the material system $G_c^{ss} = 1.36\ \mathrm{kJ/m^2}$. A scalar, γ, is introduced such that the applied ERR, G_{app}, can be expressed relative to the plateau fracture toughness as indicated here: $G_{app} = \gamma G_c^{ss}$. The applied bending moment, M_{app}, may also be expressed in terms of the scalar γ since $M^2 \propto G$ cf. Eq. (7):

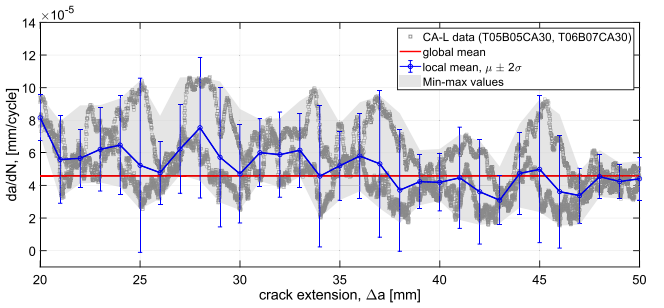

Fig. 9. Crack growth rate versus crack length of the CA30 tests. The global mean is computed as the mean value of da/dN over the entire range $a = [20; 50]$ mm. The local mean is computed within every 1 mm of crack extension which contains approximately 320–480 data points.

$M_{app} = \sqrt{\gamma} M_c^{ss}$, where the plateau moment is $M_c^{ss} = 14.98$ Nm cf. Eq. (7). The applied bending moments are listed in Tables A.1 and A.2 in Appendix A. A load ratio of $R = M_{min}/M_{max} = 0.2$ is kept in every load block of all the cyclic tests. The value ΔN_{image}, is the number of load cycles between two consecutive images during the cyclic test as explained in Section 3.4.

The CA tests are used to characterize Paris' law parameters and constitute a CA baseline measurement for analysis of transient crack growth. Constant G-tests are conduced at four different values of the maximum ERR, G_{max}, and a constant load ratio $R = 0.2$.

The two-level block loading tests are used to characterize the transient function, T_{HL}, in Eq. (5) and to investigate its' dependence on governing fatigue load parameters, i.e. item (B) in Section 1.2. The six parameters: $G_{max,L}$, $G_{max,H}$, $G_{min,L}$, $G_{min,H}$, n_L, n_H completely define the two-level block loading tests (assuming a constant frequency of the cyclic tests), cf. Fig. 1(a). It is outside the scope of the current work to characterize the effect of each parameter on the transient crack growth rate. In the two-level block loading tests the magnitude of the step change in maximum ERR, $\Delta G_{max} = G_{max,H} - G_{max,L}$, is the primary parameter under investigation. The other parameters are constrained by the following: $G_{min}/G_{max} = R^2 = 0.04$ for the H- and L-load blocks, the durations of the H- and L-load blocks are fixed at $n_H = 200$ and $n_L = 20{,}000$, respectively, and the maximum ERR of the L-load blocks are fixed at $G_{max,L} = 0.3 G_c^{ss}$. A total of four two-level block loading tests are performed as shown in Table A.1.

The results from the CA, BL, and DEM tests are presented in Section 3.6, Section 3.7 and Section 4, respectively.

3.6. CA loading and steady-state crack growth rates

Fig. 9 shows a graph of the crack growth rate versus the crack length for the constant G-tests T05B05CA30 and T06B07CA30 at $G_{max}/G_c^{ss} = 0.3$. The crack growth rate is approximately constant in both tests and is in agreement with Paris' law like expressions for the crack growth rate. The mean value of the crack growth rate is $da/dN = 4.60 \cdot 10^{-5}$ mm/cyc and is denoted as the global mean in Fig. 9. The standard deviation is on the order of $2\sigma \approx \pm 3.4 \cdot 10^{-5}$ mm/cyc.

The crack growth rates versus the maximum applied ERR are reported in Fig. 10 on log–log axes for all the constant G-tests. A nonlinear least squares fit is generated to characterize parameters of Paris' law on the following form:

$$\frac{da}{dN} = A \left(\frac{G_{max}(1-R)}{G_c^{ss}} \right)^p \tag{11}$$

Where parameters $A = 0.0727$ and $p = 5.13$ have been computed. The crack growth rates measured in the constant G-tests using the pure moment loaded DCB test configuration are steady-state responses because the crack tip propagates in a self-similar fashion at a constant crack growth rate. During steady-state crack growth, the fully

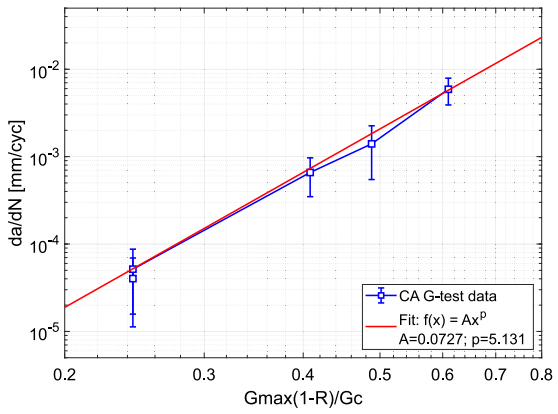

Fig. 10. Correlation between the crack growth rate, da/dN, and the maximum applied ERR, G_{max}, on double logarithmic axes. The curve fit yields the Paris' law parameters.

developed fiber bridging zone maintains its size and translates along the crack tip in a self-similar manner [22,58–60]. Consequently, the crack growth rates measured form the constant G-tests are considered as steady-state responses and are used as baseline measurements to investigate the crack growth rate under VA loading. Transient crack growth phenomena are identified when the measured crack growth rate following a load amplitude change is significantly different from the steady-state response.

3.7. Two-level block amplitude loading

The primary objective of the current section is to characterize the transient response in the crack growth rate that follows the HL load amplitude changes in two-level block loading tests. The fatigue crack growth during the two-level block loading tests is analyzed in terms of the elapsed number of load cycles, N, the average crack length, a, across the specimen width, and the crack growth rate, da/dN. Additionally, the data is divided into H- and L-load blocks and grouped depending on the load block number, i.e. the number i cf. Fig. 1(a).

For every H- and L-load block the crack extension, Δa, and the crack growth rate, da/dN, are plotted as a function of the load cycle increment ΔN following every LH- and HL load amplitude changes, respectively. This generates a series of response curves for every H- and L-load block, similar to the illustration in Fig. 1(b)–(c). Examples from the BL3075 test are provided in Fig. 11(a)–(d). The numbers on the graphs indicate the load block numbers. Figs. 11(a) and 11(c) show the responses following the LH load amplitude changes, whereas Figs. 11(b) and 11(d) shows the responses following HL load amplitude changes. Similar tendencies are observed for all the BL tests, and the observed trends are consistent with the experimental observations in [22].

It is assumed that the transient responses following the HL load amplitude changes are independent of the load block number, cf. item (d) in Section 1.1. A function on the following form is fitted to the transient crack growth response following the HL load amplitude changes:

$$da/dN = A_{0.3}\exp\left(-\frac{N-N_0}{\tau_{0.3}}\right) + \frac{da}{dN}_{ss,0.3} \tag{12}$$

The sub-index of 0.3 indicates the fixed value of $G_{max,L} = 0.3G_c^{ss}$ in all the two-level BL tests. Notice the overshoot parameter $A_{0.3}$ in Eq. (12) has units of mm/cyc, and $\tau_{0.3}$ is the decay constant. The parameter $da/dN_{ss,0.3}$ is the crack growth rate by the end of the transient phase, and is equal to the steady-state crack growth rate as measured under CA loading at $G_{max} = 0.3G_c^{ss}$. The parameter $da/dN_{ss,0.3}$ can be computed from Paris' law in Eq. (11). The resulting curve fits are presented in Fig. 12(a)–(d) for each two-level block loading test.

The transient function, T_{HL}, in Eq. (5) is defined in terms of the parameter B [−], which expresses the transient crack growth rate relative to the CA baseline value. A fraction can be computed by division of the overshoot parameter, $A_{0.3}$, and the CA baseline value, $da/dN_{ss,0.3}$, such that a parameter $B_{0.3} = A_{0.3}/da/dN_{ss,0.3}$ can be defined. The curve fitting parameters $B_{0.3}$ and $\tau_{0.3}$ obtained from the two-level BL tests are plotted against the step change in the maximum ERR between the H- and L-load blocks, $\Delta G_{max} = G_{max,H} - G_{max,L}$, in Fig. 13(a)–(b).

Linear least squares methods are used to generate a second order polynomial curve fit and a first order polynomial curve fit to describe the relationship between the parameter $B_{0.3}$ and $\tau_{0.3}$, respectively, and the step change in maximum ERR, ΔG_{max}. The resulting equations are presented in Eqs. (13) and (14). A trivial point (ΔG_{max}; $B_{0.3}$) = (0; 0) is added to the $B_{0.3}$-parameter's curve fitting data set, since no transient effect is expected for $\Delta G_{max} = 0$.

$$B_{0.3} = p_{2B}\left(\frac{|\Delta G_{max}|}{G_c^{ss}}\right)^2 + p_{1B}\left(\frac{|\Delta G_{max}|}{G_c^{ss}}\right) + p_{0B} \tag{13}$$

$p_{2B} = 20.69;\ p_{1B} = 6.80;\ p_{0B} = 0;\quad R^2 = 0.956$

$$\tau_{0.3} = p_{1\tau}\left(\frac{|\Delta G_{max}|}{G_c^{ss}}\right) + p_{0\tau} \tag{14}$$

$p_{1\tau} = -9451;\ p_{0\tau} = 10620;\quad R^2 = 0.45$

Clearly the parameter $B_{0.3}$ increases as the magnitude of the amplitude step change, ΔG_{max}, increases and the quadratic function fits the data well. The decay constant of the transient responses appears to decrease as the magnitude of the amplitude step change increases, however, the linear relationship is less evident and possesses a poor R^2-value.

3.8. Extrapolation to arbitrary load levels

The relations in Eqs. (13) and (14) for $B_{0.3}$ and $\tau_{0.3}$, respectively, are derived for a fixed maximum value of the ERR, $G_{max,L} = 0.3G_c^{ss}$, in the L-load level of the HL load amplitude changes under investigation. Manipulation of the $B_{0.3}$- and $\tau_{0.3}$-relations is necessary to generalize the trends to arbitrary H- and L-load levels of the HL load amplitude change, such that the transient function in Eq. (5) can be applied in multi-level block loading. The corresponding generalized parameters will be denoted by B and τ (without sub-index). Assumptions are necessary to avoid an immense experimental campaign.

The parameter B is assumed to be identical to $B_{0.3}$ from Eq. (13), such that:

$$B = B_{0.3} \tag{15}$$

Consequently, the B parameter for an arbitrary HL load amplitude change is only a function of the step change in maximum applied ERR $B(\Delta G_{max})$.

The decay constant, τ, is modified with respect to the decay constant $\tau_{0.3}$. The decay constant, τ, for arbitrary load levels is related to the decay constant $\tau_{0.3}$ through the relation in Eq. (16) (the reader may find details on the derivation in Appendix A.1):

$$\tau = \tau_{0.3}\left(\frac{\frac{da}{dN}_{ss,0.3}}{\frac{da}{dN}_{ss}}\right) = \tau_{0.3}\left(\frac{G_{max,L0.3}/G_c^{ss}}{G_{max,L}/G_c^{ss}}\right)^p \tag{16}$$

where $da/dN_{ss,0.3}$ represents the CA baseline crack growth rate at the L-load level that has been used to measure the decay constant $\tau_{0.3}$ in Eq. (14) from two-level block loading tests. Notice that the numerator on the right-hand side simplifies to $G_{max,L0.3}/G_c^{ss} = 0.3$ and that τ depends on $\tau_{0.3}$ and $G_{max,L}$. The effect of the multiplication in Eq. (16) is an adjustment of the transient phase's duration ($\propto \tau$). For example, the duration of the transient phase reduces when the crack growth rate da/dN_{ss} in an arbitrary L-load block is higher than $da/dN_{ss,0.3}$.

In summary, the two-level block loading tests are performed to characterize an exponential decaying function that describes the transient crack growth rate following a HL load amplitude change. The

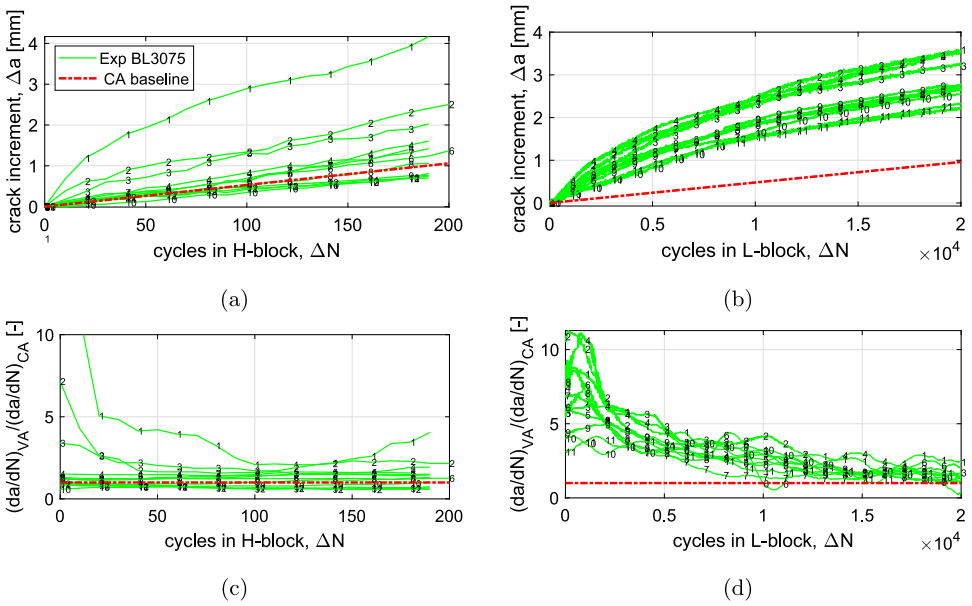

Fig. 11. Data for the BL3075 test. The crack extension, Δa, and the crack growth rate, da/dN, within an arbitrary load block is plotted against the load cycle increment, ΔN, following load amplitude change. Fig. (a) and Fig. (c) show the response curves during the H-load blocks of the BL test. Fig. (b) and Fig. (d) show the response curves during the L-load blocks of the BL test. The numbers in the graphs refer to the load block number cf. Fig. 2-1.

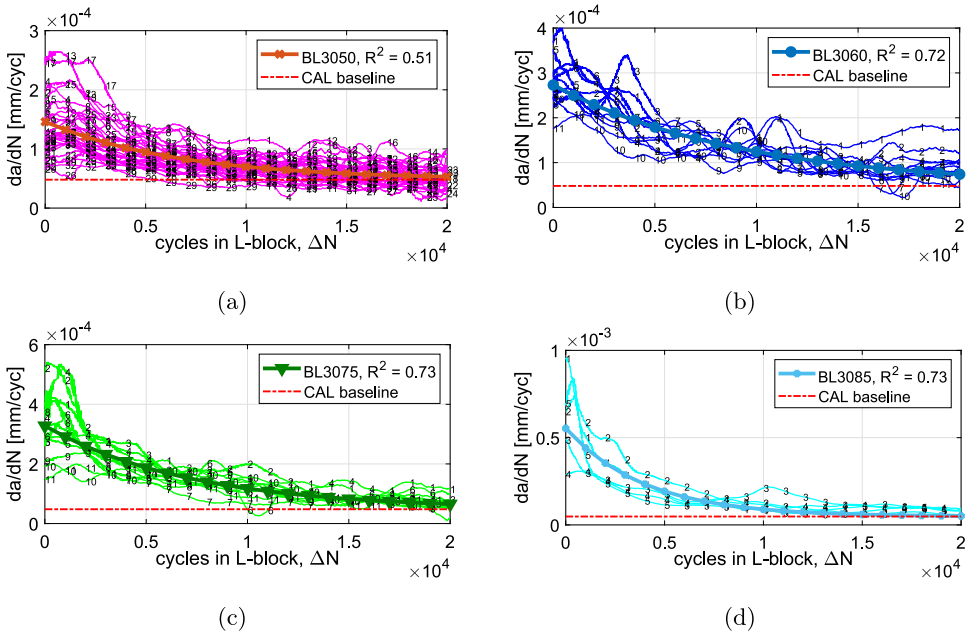

Fig. 12. Superimposing the transient crack growth rate following every HL load amplitude change in the two-level block amplitude loading tests. (a) BL3050. (b) BL3060. (c) BL3075. (d) BL3085. Least squares curve-fits are included for every test.

two-level block loading experiments also studied how the function's parameters ($B_{0.3}$ and $\tau_{0.3}$) are affected by varying ΔG_{max} while keeping $G_{max,L}$ fixed at $0.3G_c^{ss}$. The $B_{0.3}$- and $\tau_{0.3}$-relations are transferred to their corresponding generalized parameters B and τ in Eq. (15) and (16), respectively, such that the relations can be applied in the transient function, T_{HL}, in Eq. (5) to describe the crack growth rate at HL load amplitude changes with an arbitrary H- and L-load level in multi-level block loading.

4. Application to multi-level block loading

The purpose is to evaluate the performance of the new crack growth rate model for multi-level block loading and benchmark the new model compared to the conventional non-interaction crack growth rate model, cf. item *C*) in Section 1.2. The two models are used to predict the crack extension and the crack growth rate during the multi-level block loading tests DEM01 and DEM02, cf. Table A.1. The fatigue crack growth is analyzed in terms of the elapsed number of load cycles, N, the average crack length, a, across the specimen width, and the crack growth rate, da/dN. The data is divided into groups depending on the

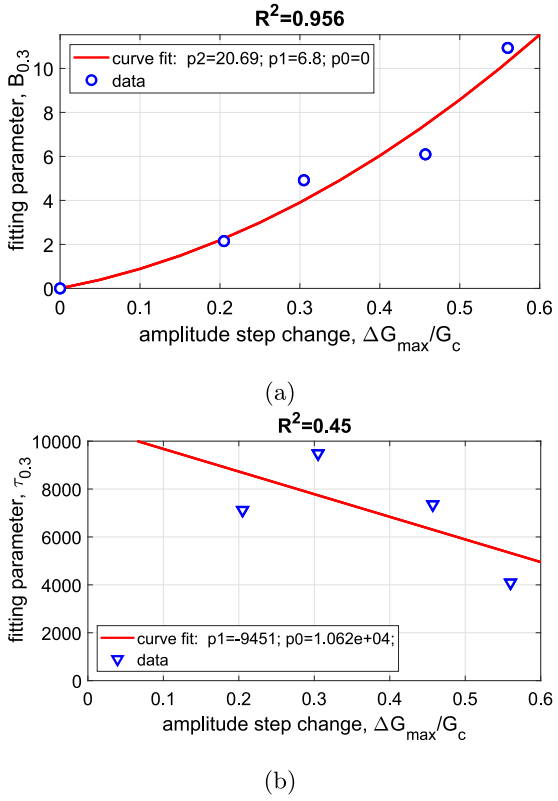

Fig. 13. (a) The relationship between the parameter B of the exponential function and the amplitude step change, $\Delta G_{max} = G_{max,H} - G_{max,L}$. (b) The relationship between the decay constant τ and the amplitude step change.

load block number to investigate the block-wise crack extension and crack growth rate. The experimental results from the demonstrator tests are presented prior to the model results.

4.1. Experimental results

The crack extension, Δa, is plotted against the number of load cycles, N, in Fig. 14(a) on the left axis, and the applied load spectrum is shown on the right axis in terms of the maximum ERR, G_{max}/G_c^{ss}. Two repetitions of the multi-level block loading test are performed. Note that a limited range of data is available for the DEM02 test as it stopped prematurely due to failure of a wire (item no. 5 in Fig. 6). The demonstrator tests DEM01 and DEM02 display similar trends. However, a relatively large difference occurs at load blocks 2–3, which cause a significant offset between the two graphs.

The crack extension, Δa, within each load block is analyzed as shown in the bar chart in Fig. 14(b). Large crack extensions occur in the early load blocks: 2, 3, 5, 6, 8 and 9, which all have a relative high value of the applied maximum ERR $G_{max}/G_c^{ss} \geq 0.6$ compared to the remaining blocks in the applied load spectrum. Although load block pairs 2–3 and 5–6 are identical, there is a difference in the amount of crack growth. The early load blocks (2,3) cause more crack extension than later load blocks (5,6,8,9). This observation is consistent with the results from the two-level block loading tests and the item *(b)* in Section 1.1.

The crack growth rate, da/dN, is shown in Fig. 14(c). The crack growth rate has been normalized with respect to the CA baseline value, i.e. the value obtained from Paris' law in Eq. (11). Hence, a value of $(da/dN_{VA})/(da/dN_{CA}) = 1$ corresponds to a crack growth rate equal to the CA baseline. Generally, the crack growth rate is higher during the VA test compared to the CA baseline. In several of the load blocks that follow HL load amplitude changes, e.g. no. 4, 7 and 21, the crack growth rate is more than a factor of five times the CA baseline value, and the crack growth rate does not reach the CA baseline value before the next load amplitude change occurs.

The tests show the characteristic exponential decay-type response at several HL load amplitude changes in Fig. 14(c), which is similar to the responses observed in the two-level block loading tests. Additionally, the crack growth rate following a given HL-load amplitude change increases as the step change ΔG_{max} increases, which is also consistent with the results in Fig. 13(a) and the two-level block loading tests.

4.2. Model results

Results from the conventional non-interaction crack growth rate model and the new interaction model are included in Fig. 14(a)–(c). The non-interaction model yields a significant error in the crack growth prediction. By the end of the test at $N_{tot} = 110,150$ load cycles, the non-interaction model has a percentage deviation of -39.4% compared to the actual crack extension measured in the VA experiment. This number may be interpreted as an average measure of the load interaction effect for the complete load spectrum.

The predicted block-wise crack extension is shown in Fig. 14(b). In every load block, the crack extension in the VA test is larger than the value computed from the non-interaction model. A significant discrepancy between the VA experiment and the non-interaction model occurs during load blocks 2–8. Several of the remaining load blocks (no. 9–26) also cause a significant difference, e.g. load block numbers 9, 10, 11, 14, 17, 19, and 21, which are mainly load blocks that follow a HL-load amplitude change. The crack extension at load block no. 21 causes a notable error. The error produced by the non-interaction model increases in regions of the load spectrum where a large variation in the maximum applied ERR, ΔG_{max}, occurs. This trend is consistent with the observations in two-level block loading (e.g. Fig. 13); the larger the step change in load level, the more significant the transient behavior becomes.

The crack growth rate as computed from the non-interaction model yields a very poor representation of the crack growth rate in the VA test as seen in Fig. 14(c).

The new interaction crack growth rate model reduces the error in crack extension between the VA test and model prediction. The new model yields a percentage deviation of -21.1% in the total crack extension compared to the VA experiment DEM01. The new model still under-predicts the crack extension compared to the VA experiment, however, the new model nearly halved the error (-21.1%) compared to the non-interaction model (-39.4%).

The new crack growth rate model provides a good representation of the crack growth rate during the load blocks that follows HL load amplitude changes, as seen in Fig. 14(c). The transient crack growth rates are well-captured by the exponential decay functions, and the prediction fits well with respect to the amount of overshoot and the rate of decay of the transient responses.

5. Discussion

5.1. Assessment of model capability and limitation

The new crack growth rate model improves the crack growth prediction compared to the non-interaction model, and it captures well the transient crack growth rate that follows HL load amplitude changes. Nevertheless, an error remains in terms of the total crack extension by the end of the multi-level block loading test, as seen in Fig. 14(a). The purpose of the multi-level block loading test is to demonstrate when and why the current modeling approach succeeds and/or fails, cf. item *(C)* in Section 1.2, which will be elaborated here.

Fig. 15 shows the error in crack increment between the model predictions and the experiment DEM01, $\epsilon_{\Delta a,i} = a_{EXP,i} - a_{PRED,i}$, for

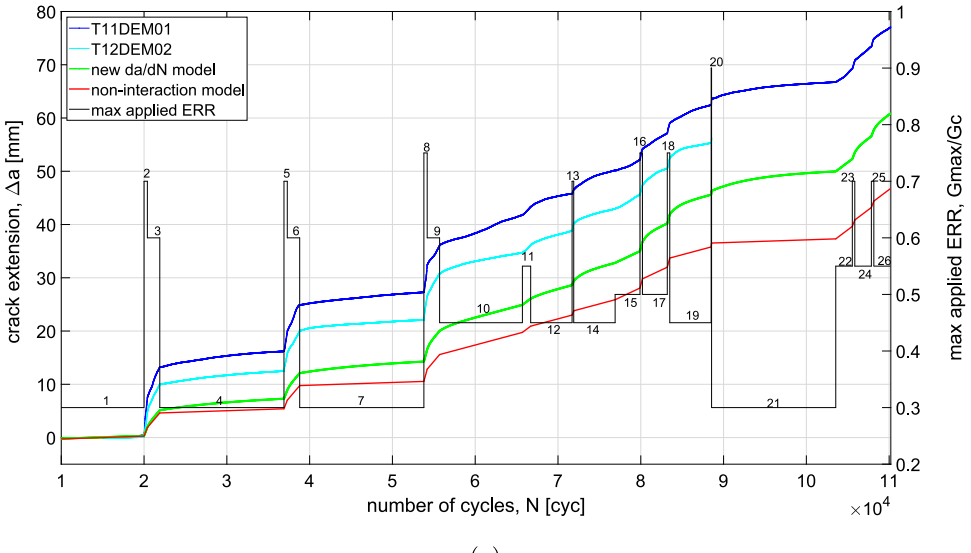

(a)

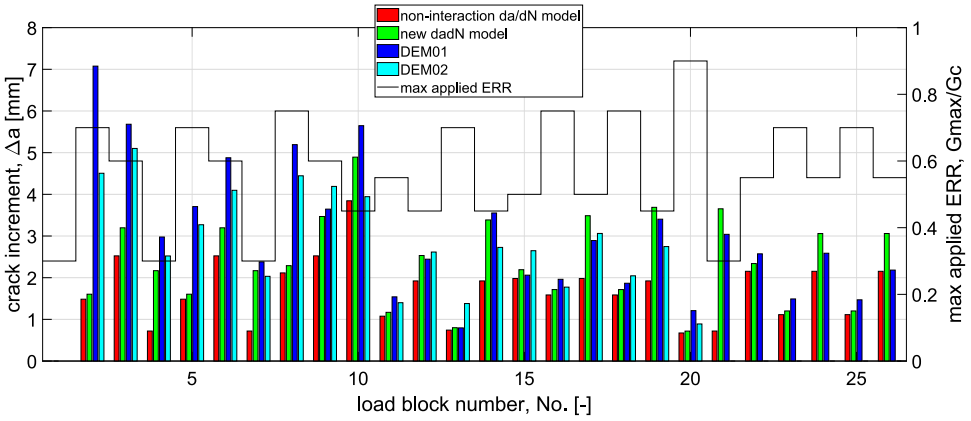

(b)

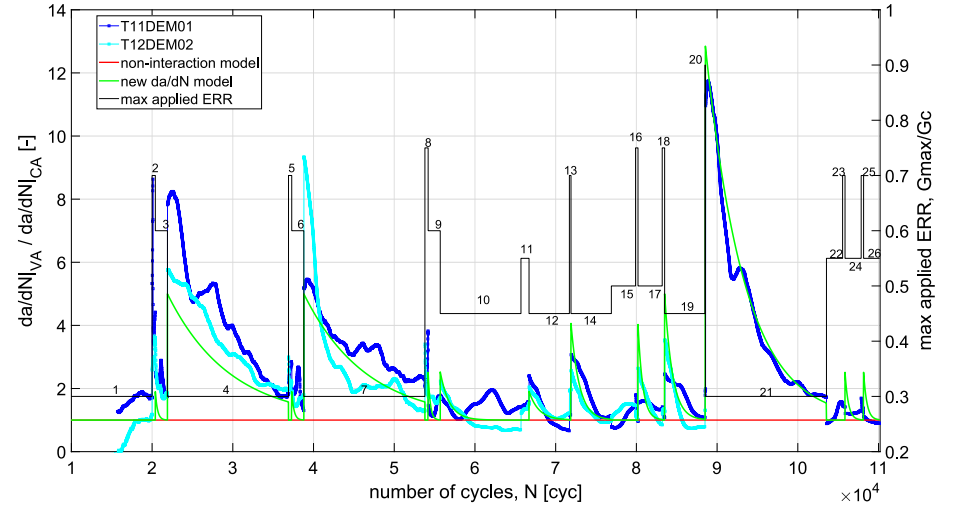

(c)

Fig. 14. (a) Left axis: Crack extension, Δa, versus the number of load cycles in the multi-level block loading test. Right axis: The maximum applied ERR (target) normalized with respect to the fracture toughness, G_c^{ss}. (b) Crack extension, Δa, within the individual load blocks versus the load block number. (c) The crack growth rate versus the number of load cycles in the multi-level block loading test. The measured crack growth rate, da/dN_{VA}, has been normalized with respect to the CA baseline crack growth rate, da/dN_{CA}, as obtained by Paris law.

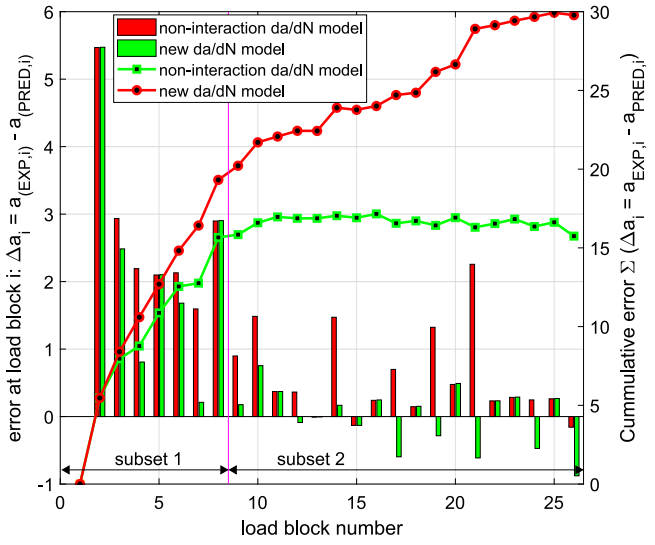

Fig. 15. Left axis: Error in crack extension of the model predictions in comparison to the non-interaction model for every load block number. Right axis: Cumulative error in crack extension.

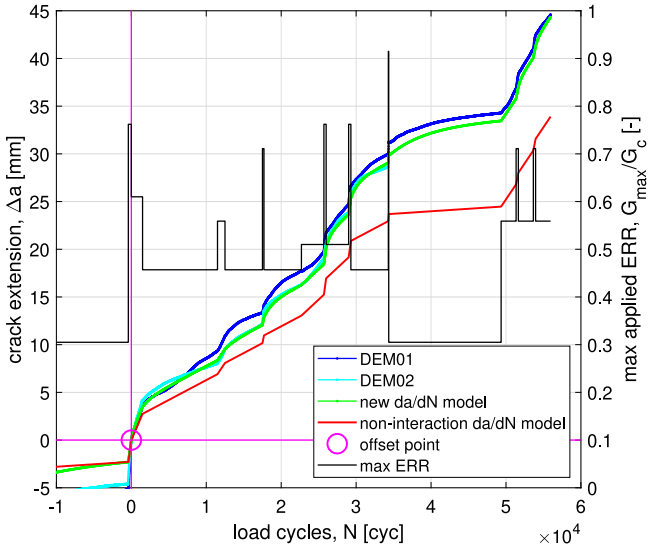

Fig. 16. Offset crack length versus number of load cycles for subset 2 (i.e. load block no. 9 to 26) of the multi-level block loading test.

every load block number. Fig. 15 also shows the cumulative model error $\sum(a_{EXP,i} - a_{PRED,i})$ on the right axis.

The load spectrum is divided into two subsets as indicated in Fig. 15, where subset 1 includes load blocks 2–8 and subset 2 includes load blocks 9–26. By the end of subset 1, the cumulative error is 19.3 mm and 15.7 mm for the conventional non-interaction model and the new interaction model, respectively. The new model gives only a slight improvement in subset 1 (particularly the error reduction in load block no. 4 and 7). The capability of the new model depends on the characteristics of the applied load spectrum. The crack growth in subset 1 is governed by load blocks with high values of G_{max} (e.g. load blocks: 2, 3, 5, 6, 8 and 9), and much of the crack growth occurs within load blocks that follow LH load amplitude changes. Observations from two-level block loading tests show that LH load amplitude changes may cause a significant increase in the crack growth rate, mainly if the LH load amplitude change occurs early in the block loading spectrum, cf. item *(b)* in Section 1.1. In this context, *early* H-load blocks refers to H-load blocks that follow steady-state crack growth at a L-load level as in the beginning of the two-level block loading tests. As the transient effects due to LH load amplitude changes are neglected in the new model, an error is expected in subset 1.

A significant reduction of the error is observed in subset 2 for the new model in comparison the non-interaction model. This is clear from the slope of the cumulative error curve, which is close to zero throughout subset 2. The crack growth in subset 2 is less affected by the LH load amplitude changes, and the new model accurately represent the crack growth rate following the HL load amplitude changes. The load block numbers 10, 12, 14, 17, 19, and 21 show a significant reduction of the error. In certain load blocks, e.g. load block number 26, the new crack growth rate model predicts too much crack extension.

A crack growth prediction for subset 2 of the multi-level block loading test is shown in Fig. 16. The new crack growth rate model provides a good representation of the $(N, \Delta a)$-graph and illustrates the capability of the new model to predict crack extension under multi-level block loading.

5.2. Model considerations

The new crack growth rate model relies on additional model parameters that are characterized by simple block loading experiments in comparison to the conventional non-interaction model. Fortunately, several trends derived from simple two-level block loading experiments also apply in the more complex multi-level block loading experiments as mentioned in Section 3.7. Assumptions, like the ones introduced in Section 3.8, are necessary to reduce the experimental campaign to manageable sizes. However, the current work has investigated a minor fraction of the many possible combinations of fatigue load parameters that define the two-level block loading experiment. The multi-level block loading experiments test some of these assumptions, e.g. the assumption in Eq. (16) related to the rate of decay of the transient response at arbitrary load levels and the assumption that the transient response is independent of the load block duration. Other fatigue load parameters have not been investigated further, e.g. the load ratio is assumed to be constant $R = 0.2$ during all the tests and the study is limited to pure mode I crack opening.

It is worth to mention that Paris' law relations depend on the fiber bridging zone, and there is no general agreement on how to include bridging effects in Paris' law relations. Bridging fibers are well-established to exert a crack tip shielding effect that reduces the fatigue crack growth rate. This is sometimes expressed as $G_{tot} = G_{tip} + G_{fb}$, where G_{tot} is the total external ERR, G_{tip} is the actual ERR experienced at the crack tip, and G_{fb} represents a crack tip shielding effect exerted by the fiber bridging zone [61–66]. The presented work has only considered the total external ERR, G_{tot}. The Paris' law in Eq. (11) has been derived from constant G-tests and the corresponding crack growth rates have been measured during steady-state crack growth, see the definition in Section 3.6. The steady-state fatigue crack growth measured in a constant G-test (at given maximum and minimum values) must imply that the crack tip shielding effect, G_{fb}, is constant in the test when the fracture process zone is fully-developed. The model parameters A and p in Eq. (11) may be different if the Paris' law is measured with the widely used DCB specimen subjected to transverse forces under CA loading in displacement- or force control, which does not enable steady-state fatigue crack growth.

The authors believe that physical-based models of the governing mechanisms in the fracture process zone and their interaction with the crack tip propagation are necessary to generalize delamination prediction models to VA spectrum loading. However, there is no consensus nor a sound understanding on how the crack tip shielding effect of the fiber bridging zone, or other underlying mechanisms, are affected by VA loading [19–21,23,66]. The new model proposed in the current work obviously lacks such physical considerations. The new model is a phenomenological approach in the sense that the transient responses are not derived from physical theories in which the actual

physical processes on a meso-/microscopic level that cause transient crack propagation are integrated. Instead, the phenomenological model ignores the underlying mechanisms and concentrates on the gross macroscopic crack tip propagation through empirical relations that are expressed in terms of physical parameters such as the ERR. The model is capable to represent important phenomenological characteristics of the crack growth behavior under multi-level block loading. In that sense, the new model also brings value as a suitable benchmark for future physics-based models.

6. Conclusion

A new crack growth rate model with transient effects has been formulated, experimentally characterized, and applied to multi-level block loading. The conclusion revisits the tasks *(A)–(C)* described in Section 1.2.

(A) The new crack growth rate model computes the current crack growth rate as the sum of two terms. The first term is a non-interaction term that can be evaluated from the instantaneous values of the cyclic load parameters, e.g. the current value of the maximum ERR, G_{max}, and the load ratio, R. This term is identical to the conventional Paris' law-like crack growth rate model. The second term is an exponential decaying function that acts as a transient term and becomes non-zero whenever a HL load amplitude change occurs in the load spectrum. The second term is a load interaction term since it depends on the load history, specifically the number of load cycles since the load amplitude change occurred and the magnitude of the step change in maximum ERR between two consecutive load blocks.

(B) The transient response is described by an exponential decay function with two model parameters: B and τ. The B parameter determines the initial overshoot in crack growth rate at the load amplitude change and is a scaling factor applied to the CA baseline crack growth rate. The decay constant τ determines the rate of decay of the transient function. The model parameters are derived from two-level block loading experiments that are completely defined from several fatigue load parameters, such as the maximum and minimum values of the ERR at the H- and L- load blocks, respectively, and the duration of the H- and L-load blocks. The step change in maximum ERR, ΔG_{max} is assumed to be the governing factor and relationships between ΔG_{max} and the model parameters B and τ are derived. Additional assumptions have been introduced to generalize the relationships.

(C) Multi-level block loading experiments are performed with a new experimental setup that enables cyclic crack growth with real-time control of the applied ERR in VA loading, and automated and precise measurements of the crack length. The experiment has provided unique and unprecedented crack growth rate measurements during multi-level block loading that is highly suited for assessing the performance of new crack growth rate models. The multi-level block loading tests demonstrate the capabilities and limitations of the new crack growth rate model. The performance is shown to depend on certain characteristics of the applied load spectrum. The early LH-load amplitude changes may cause a significant increase in the crack extension that is not included in the current model. However, the new crack growth rate model accurately represents the crack growth rate following the HL load amplitude changes in the multi-level block loading test, and yields a significant reduction in the error compared to a non-interaction model, which the vast majority of state-of-the-art delamination models are based upon.

Finally, the experimental data and the new model generate important phenomenological characteristics of the crack growth behavior under multi-level block loading, that future physics-based models are challenged to predict. The experimental data from the multi-level block loading experiments is available, see Data availability section below.

Declaration of competing interest

The authors declare the following financial interests/personal relationships which may be considered as potential competing interests: Simon Mosbjerg Jensen reports financial support was provided by European Union's Horizon 2020.

Data availability

The experimental data required to reproduce the multi-level block loading tests are available to download from (http://dx.doi.org/10.17632/gj69dy4pcp.1), an open-source online data repository hosted at Mendeley Data [67].

Acknowledgment

This project has received funding from the European Union's Horizon 2020 research and innovation programme under grant agreement No. 763990.

Appendix A

A.1. Correction of decay constant

This section provides additional information on the correction applied to the decay constant in Eq. (16). The crack growth following a HL load amplitude change is considered, such that the crack growth rate da/dN is described by Eqs. (1) and (3)–(5). It is assumed that the transient phase is finite and completed when $da/dN = 1.01 da/dN_{ss}$. The load cycle increment associated with the transient phase, ΔN_τ, then becomes:

$$\frac{da}{dN}_{ss}\left(1 + B\exp\left(\frac{-\Delta N_\tau}{\tau}\right)\right) = 1.01\frac{da}{dN}_{ss} \Leftrightarrow$$
$$\Delta N_\tau = \tau \ln\left(\frac{B}{0.01}\right) \tag{A.1}$$

The crack increment, Δa_τ, associated with the transient phase can then be computed by substitution of ΔN_τ into Eq. (6):

$$\Delta a_\tau = \frac{da}{dN}_{ss}\left(\Delta N_\tau + B\tau\left(1 - \exp\left(\frac{-\Delta N_\tau}{\tau}\right)\right)\right) \Leftrightarrow$$
$$\Delta a_\tau = \frac{da}{dN}_{ss}\alpha(B)\tau \tag{A.2}$$

where $\alpha(B) = \ln(B/0.01) + B - 0.01$, and the steady-state crack growth rate, da/dN_{ss}, can be computed from Eq. (3). The steady-state crack growth rate attains a constant value in a given load block. Rewriting of Eq. (A.2) enables one to write the decay constant τ as:

$$\tau = \frac{\Delta a_\tau}{\frac{da}{dN}_{ss}\alpha(B)} \tag{A.3}$$

The decay constant that is derived from experiments in Section 3.7 is based on crack growth rate measurements during a L-load block at which $G_{max,L} = 0.3G_c^{ss}$. This decay constant has been denoted as $\tau_{0.3}$. The correction applied to the decay constant in Section 3.8 ensures that the decay constant makes sense for arbitrary load levels of the L-load block. The decay constant for arbitrary load levels will be denoted by τ. The ratio between the reference and arbitrary decay constants, $\tau_{0.3}$ and τ, respectively, then becomes:

$$\frac{\tau}{\tau_{0.3}} = \frac{\Delta a_\tau}{\Delta a_{\tau,0.3}}\frac{\alpha(B_{0.3})}{\alpha(B)}\frac{\frac{da}{dN}_{ss,0.3}}{\frac{da}{dN}_{ss}} \tag{A.4}$$

Using Eq. (3) the following expression can be derived:

$$\frac{\tau}{\tau_{0.3}} = \frac{\Delta a_\tau}{\Delta a_{\tau,0.3}}\frac{\alpha(B_{0.3})}{\alpha(B)}\left(\frac{G_{max,L0.3}/G_c^{ss}}{G_{max,L}/G_c^{ss}}\right)^p \tag{A.5}$$

Table A.1
Test matrix showing the test ID and the applied load pattern. The parameter ΔN_{im} is the cycle increment for crack length measurements.

Test ID	$\gamma_{max,L}$	$\gamma_{max,H}$	Applied moment, $\mathbf{M_{app}}$ [Nm], R=0.2	$\mathbf{\Delta N_{im}}$ [cyc]
T01B03BL3060	0.305	0.610	$M_{max,L} = 8.27$; $M_{max,H} = 11.70$;	10
T02B02BL3075	0.305	0.762	$M_{max,L} = 8.27$; $M_{max,H} = 13.08$;	10
T05B05CA30	0.305	–	$M_{max} = 8.27$;	100
T06B07CA30	0.305	–	$M_{max} = 8.27$;	100
T07B10BL3050	0.305	0.510	$M_{max,L} = 8.27$; $M_{max,H} = 10.70$;	10
T08B09CA50	0.510	–	$M_{max} = 10.70$;	50
T09B04CA60	0.610	–	$M_{max} = 11.70$;	20
T10B06CA75	0.762	–	$M_{max} = 13.08$;	10
T11B05DEM01	–	–	–	10
T12B02DEM02	–	–	–	10
T13B08BL3085	–	0.864	$M_{max,L} = 8.27$; $M_{max,H} = 13.92$;	10

Table A.2
Details on the applied multi-level block loading spectrum.

Load block number	$\gamma_{max} = \mathbf{G_{max}/G_c^{ss}}$	$\mathbf{M_{max}}$ [Nm], R = 0.2	Number of load cycles, $\mathbf{N_i}$ [cyc]
1	0.305	8.27	20,000
2	0.711	12.63	400
3	0.610	11.70	1,500
4	0.305	8.27	15,000
5	0.711	12.63	400
6	0.610	11.70	1,500
7	0.305	8.27	15,000
8	0.762	13.08	400
9	0.610	11.70	1,500
10	0.457	10.13	10,000
11	0.559	11.20	1,000
12	0.457	10.13	5,000
13	0.711	12.63	200
14	0.457	10.13	5,000
15	0.510	10.70	3,000
16	0.762	13.08	300
17	0.510	10.70	3,000
18	0.762	13.08	300
19	0.457	10.13	5,000
20	0.915	14.33	50
21	0.305	8.27	15,000
22	0.559	11.20	2,000
23	0.711	12.63	300
24	0.559	11.20	2,000
25	0.711	12.63	300
26	0.559	11.20	2,000
Total cycles:			110,150

Although the crack increment, Δa_τ, associated with the transient phase and the function $\alpha(B)$ will vary depending on the applied load level, the final factor in Eq. (A.4) proves to be the governing factor by two orders of magnitude. It is therefore reasonable to omit the first and second factor in Eq. (A.5) such that the equation reduces to Eq. (16) in Section 3.8.

A.2. Test matrix

Table A.1 provides an overview of the test programme. Table A.2 provides details on the load spectrum applied in the demonstrator tests DEM01 and DEM02.

References

[1] Mishnaevsky LJ. Root causes and mechanisms of failure of wind turbine blades: Overview. Materials 2022;15:2959.

[2] Jensen PH, Fugleberg K. Wind energy research strategy. report, Danish Research Consortium for Wind Energy, www.DFFV.dk; 2015.

[3] McGugan M, Pereira G, Sørensen BF, Toftegaard H, Branner K. Damage tolerance and structural monitoring for wind turbine blades. Phil Trans R Soc A 2015;373:2014007.

[4] Degrieck J, Van Paepegem W. Fatigue damage modeling of fibre-reinforced composite materials: Review. Appl Mech Rev 2001;54(4):279–300.

[5] Hwang W, Han KS. Cumulative damage models and multi-stress fatigue life prediction. J Compos Mater 1986;20:125–53.

[6] Farrow IR. Damage accumulation and degradation of composite laminates under aircraft service loading: assessment and prediction, volumes I and II [Ph.D. thesis], Cranfield Institute of Technology; 1998.

[7] Broutman LJ, Sahu S. A new theory to predict cumulative fatigue damage in fiberglass reinforced plastics. In: Composite materials. testing and design, ASTM STP 497. 1972, p. 170–88.

[8] Hashin Z. Cumulative damage theory for composite materials: Residual life and residual strength methods. Compos Sci Technol 1985;23:1–19.

[9] Yang JN, Jones DL. Load sequence effects on the fatigue of unnotched composite materials. In: Fatigue of fibrous composite materials, ASTM STP, Vol. 723. 1981, p. 213–32.

[10] Schaff JR, Davidson BD. Life prediction methodology for composite structures part I - Constant amplitude and two-stress level fatigue. J Compos Mater 1997;31(2):128–57.

[11] Schaff JR, Davidson BD. Life prediction methodology for composite structures part II - spectrum fatigue. J Compos Mater 1997;31(2):158–81.

[12] Van Paepegem W, Degrieck J. Effects of load sequence and block loading on the fatigue response of fiber-reinforced composites. Mech Adv Mater Struct 2002;9(1):19–35.

[13] Bartley-Cho J, Lim SG, Hahn HT, Shyprykevich P. Damage accumulation in quasi-isotropic graphite/epoxy laminates under constant-amplitude fatigue and block loading. Compos Sci Technol 1998;58:1535–47.

[14] Gamstedt EK, Sjøgren BA. An experimental investigation of the sequence effect in block amplitude loading of cross-ply composite laminates. Int J Fatigue 2002;24:437–46.

[15] Ogi K, Yashiro S, Niimi K. A probabilistic approach for transverse crack evolution in a composite laminate under variable amplitude cyclic loading. Composites A 2010;41,3:383–90.

[16] Glud JA, Dulieu-Barton JM, Thomsen OT, Overgaard LCT. Fatigue damage evolution in GFRP laminates with constrained off-axis plies. Composites A 2017;95:359–69.

[17] Bender JJ, Bak BLV, Jensen SM, Lindgaard E. Effect of variable amplitude block loading on intralaminar crack initiation and propagation in multidirectional GFRP laminate. Composites B 2021;217:108905.

[18] Erpolat S, Ashcroft IA, Crocombe AD, Abdel-Wahab MM. Fatigue crack growth acceleration due to intermittent overstressing in adhesively bonded CFRP joints. Composites A 2004;35:1175–83.

[19] Yao L, Sun Y, Zhao M, Alderliesten RC, Benedictus R. Stress ratio dependence of fibre bridging significance in mode I fatigue delamination growth of composite laminates. Composites A 2017;95:65–74.

[20] Androuin G, Michel L, Maillet I, Gong X. Characterization of fatigue delamination growth under mode I and mode II: Effects of load ratio and load history. Eng Fract Mech 2018;203:172–85.

[21] Jensen SM, Bak BLV, Bender JJ, Lindgaard E. Transition-behaviours in fatigue-driven delamination of GFRP laminates following step changes in block amplitude loading. Int J Fatigue 2021;144:106045.

[22] Jensen SM, Bak BLV, Bender JJ, Carreras L, Lindgaard E. Transient delamination growth in GFRP laminates with fibre bridging under variable amplitude loading in G-control. Composites B 2021;225:109296.

[23] Sarfaraz R, Vassilopoulos AP, Keller T. Block loading fatigue of adhesively bonded pultruded GFRP joints. Int J Fatigue 2013;49:40–9.

[24] Sarfaraz R, Vassilopoulos AP, Keller T. Variable amplitude fatigue of adhesively-bonded pultruded GFRP joints. Int J Fatigue 2013;55:22–32.

[25] Sendeckyj G. Life prediction for resin-matrix composite materials. In: Reifsnider KL, editor. Fatigue of composite materials. Composite material series, vol 4, Elsevier; 1990, p. 431–83.

[26] Post NL, Case SW, Lesko JJ. Modeling the variable amplitude fatigue of composite materials: A review and evaluation of the state of the art for spectrum loading. Int J Fatigue 2008;30:2064–86.

[27] Vassilopoulos AP. Fatigue life prediction of composite materials under realistic loading conditions (variable amplitude loading), Vol. Chapt. 9. Woodhead Publishing; 2010, p. 293–333.

[28] Bak BLV, Sarrado C, Turon A, Costa J. Delamination under fatigue loads in composite laminates: A review on the observed phenomenology and computational methods. Appl Mech Rev 2014;66:1–24.

[29] Barenblatt GI. Concerning equilibrium cracks forming during brittle fracture: The stability of isolated cracks. J Appl Math Mech 1959;23:622–36.

[30] Dugdale DS. Yielding of steel sheets containing slits. J Mech Phys Solids 1960;8(2):100–4.

[31] Ortiz M, Pandolfi A. Finite-deformation irreversible cohesive elements for three-dimensional crack-propagation analysis. Internat J Numer Methods Engrg 1999;44(9):1267–82.

[32] Alfano G, Crisfield MA. Finite element interface models for the delamination analysis of laminated composites: Mechanical and computational issues. Internat J Numer Methods Engrg 2001;50(7):1701–36.

[33] Camanho PP, Dávila CG, de Moura MF. Numerical simulation of mixed-mode progressive delamination in composite materials. J Compos Mater 2003;37(16):1415–38.

[34] Turon A, Camanho PP, Costa J, Dávila CG. A damage model for the simulation of delamination in advanced composites under variable-mode loading. Mech Mater 2006;38(11):1072–89.

[35] Lindgaard E, Bak BLV, Glud JA, J. S, Christensen ET. A user programmed cohesive zone finite element for ANSYS mechanical. Eng Frac Mech 2017;38(11):1072–89.

[36] Jensen SM, Martos MJ, Bak BLV, Lindgaard E. Formulation of a mixed-mode multilinear cohesive zone law in an interface finite element for modelling delamination with R-curve effects. Compos Struct 2019;216:477–86.

[37] Maiti S, Geubelle PH. A cohesive zone model for fatigue failure of polymers. Eng Fract Mech 2005;72(5):691–708.

[38] Roe KL, Siegmund T. An irreversible cohesive zone model for interface fatigue crack growth simulation. Eng Fract Mech 2003;70:209–32.

[39] Robinson GI, Galvanetto U, Tumino D, Bellucci G, Violeau D. Numerical simulation of fatigue-driven delamination using interface elements. Internat J Numer Methods Engrg 2005;63(13):1824–48.

[40] Tumino D, Cappello F. Simulation of fatigue delamination growth in composites with different mode mixtures. J Compos Mater 2007;41(20):2415–41.

[41] Turon A, Costa J, Camanho PP, Dávila CG. Simulation of delamination in composites under high-cycle fatigue. Compos Part A 2007;38(11):2270–82.

[42] Harper PW, Hallet SR. A fatigue degradation law for cohesive interface elements—Development and application to composite materials. Int J Fatigue 2010;32(11):1774–87.

[43] Krueger R. Development of benchmark examples for static delamination propagation and fatigue growth predictions. Tech. rep., Langley Research Center; 2011, Technical Report No. NASA/NF-1676L-11493.

[44] Yang B, Mall S, Ravi-Chandar K. A cohesive zone model for fatigue crack growth in quasi-brittle materials. Int J Solid Struct 2001;38(22-23):3927–44.

[45] Turon A, Bak BLV, Lindgaard E, Sarrado C, Lund E. 3 - interface elements for fatigue-driven delaminations in advanced composite materials. In: Hallett PP, Camanho SR, editors. Numerical modelling of failure in advanced composite materials. Woodhead publishing series in composites science and engineering, Woodhead Publishing; 2015, p. 73–91.

[46] Bak BLV, Turon A, Lindgaard E, Lund E. A simulation method for high-cycle fatigue-driven delamination using a cohesive zone model. Internat J Numer Methods Engrg 2016;106(3):163–91. http://dx.doi.org/10.1002/nme.5117.

[47] Bak BLV, Turon A, Lindgaard E, Lund E. A benchmark study of simulation methods for high-cycle fatigue-driven delamination based on cohesive zone models. Compos Struct 2017;164:198–206. http://dx.doi.org/10.1016/j.compstruct.2016.11.081.

[48] Carreras L, Turon A, Bak BLV, Lindgaard E, Renart J, Martin de la Escalera F, et al. A simulation method for fatigue-driven delamination in layered structures involving non-negligible fracture process zones and arbitrarily shaped crack fronts. Composites A 2019;122:107–19.

[49] Tao C, Mukhopadhyay S, Zhang B, Kawashita LF, Qiu J, Hallet SR. An improved delamination fatigue cohesive interface model for complex three-dimensional multi-interface cases. Compos Part A: Appl Sci Manuf 2018;107:633–46.

[50] Llobet J, Maimí P, Turon A, Bak B, Lindgaard E, Carreras L, et al. A continuum damage model for composite laminates: Part IV- experimental and numerical tests. Mech Mater 2021;154.

[51] Trabal GG, Bak BLV, Chen B, Carreras L, Lindgaard E. An adaptive floating node based formulation for the analysis of multiple delaminations under high cycle fatigue loading. Composites A 2022;160:107036.

[52] Carreras L, Bak BLV, Jensen SM, Lequesne C, Xiong H, Lindgaard E. Benchmark test for mode I fatigue-driven delamination in GFRP composite laminates: Experimental results and simulation with the inter-laminar damage model implemented in SAMCEF. Composites B 2023;253:110529.

[53] Suo Z. Delamination specimens for orthotropic materials. J Appl Mech 1990;57:627–734.

[54] Hutchinson JW, Suo Z. Mixed mode cracking in layered materials. Adv Appl Mech 1992;29:63–191.

[55] Sørensen BF, Jørgensen K, Jacobsen TK, Østergaard RC. DCB-specimen loaded with uneven bending moments. Int J Fract 2006;141:163–76.

[56] Dessureault M, Spelt JK. Observations of fatigue crack initiation and propagation in an epoxy adhesive. Int J Adhesion Adhesives 1996;17:183–95.

[57] Bak BLV, Lindgaard E. A method for automated digital image-based tracking of delamination fronts in translucent glass fibre-laminated composite materials. Strain 2020.

[58] Sørensen BF. Delamination fractures in composite materials. In: Talreja A, Varna J, editors. Modeling damage, fatigue and failure of composite materials. Woodhead Publishing Series in Composites Science and Engineering: Number 65; 2016.

[59] Suo Z, Bao G, Fan B. Delamination R-curve phenomena due to damage. J Mech Phys Solids 1992;40:1–16.

[60] Holmes JW, Liu L, Sørensen BF, Wahlgren S. Experimental approach for mixed-mode fatigue delamination crack growth with large-scale bridging in polymer composites. J Compos Mater 2014;48(25):3111–28.

[61] Hojo M, Ochiai S, Aoki T, Ito H. Mode I fatigue delamination for CF/PEEK laminates using maximum-energy-release-rate constant tests. J Soc Mat Sci Jpn 1995;44:953–9.

[62] Gregory JR, Spearing SM. A fiber bridging model for fatigue delamination in composite materials. Acta Mater 2004;52:5493–502.

[63] Donough MJ, Gunnion AJ, Orifici AC, Wang CH. Scaling parameter for fatigue delamination growth in composites under varying load ratios. Compos Sci Technol 2015;120:39–48.

[64] Farmand-Ashtiani E, Cugnoni J, Botsis J. Effects of large scale bridging in load controlled fatigue delamination of unidirectional carbon-epoxy specimens. Compos Sci Technol 2016;137:52–9.

[65] Yao L, Sun Y, Guo L, Zhao M, Jia L, Alderliesten RC, et al. A modified Paris relation for fatigue delamination with fibre bridging in composite laminates. Compos Struct 2017;176:556–64.

[66] Jensen SM, Bak BLV, Lindgaard E, Renart J. Micromechanisms of load history effects in fatigue-driven delamination growth. In: 8th ECCOMAS thematic conference on the mechanical response of composites composites 2021. Gothenburg Sweden; 2021.

[67] Jensen SM, Carreras L, Bak BLV, Lequesne C, Lindgaard E. Experimental data set for: A crack growth rate model with load history effects for mode I fatigue-driven delamination under multi-level block loading. Mendeley Data 2023. URL http://dx.doi.org/10.17632/gj69dy4pcp.1.